Research Square

Preprints are preliminary reports that have not undergone peer review.
They should not be considered conclusive, used to inform clinical practice,
or referenced by the media as validated information.

Theoretical and Experimental Study on Anti-Penetration Performance of Water-Bearing Nano-Quartz Sand Composite Targets Against Shaped Charge Jets

H Wang
Nanjing University of Science and Technology
S. W. Chen
csw-6070@njust.edu.cn
Nanjing University of Science and Technology
M Xia
State Key Laboratory of Target Vulnerability Assessment, Defense Engineering Institute, Academy of Military Science, People's Liberation Army
Z. G. Ding
Jiangnan Industry Group Co., Ltd

Article

Keywords: Shaped charge jet, Nano-quartz sand composite target, Moisture content, Penetration resistance

Posted Date: November 24th, 2026

DOI: https://doi.org/10.21203/rs.3.rs-11609432/v1

License: This work is licensed under a Creative Commons Attribution 4.0 International License.
Read Full License

Additional Declarations: No competing interests reported.

Theoretical and Experimental Study on Anti-Penetration Performance of Water-Bearing Nano-Quartz Sand Composite Targets Against Shaped Charge Jets

H Wang [1], S.W. Chen [1*], M Xia [2*], Z.G. Ding [3]

[1]Nanjing University of Science and Technology, Nanjing, Jiangsu, China.

[2]State Key Laboratory of Target Vulnerability Assessment, Defense Engineering Institute, Academy of Military Science, People's Liberation Army Luoyang, China.

[3]Jiangnan Industry Group Co., Ltd., Xiangtan, Hunan, China

Email: csw-6070@njust.edu.cn, xiaming052021@163.com

Abstract

Particle-filled composite armor has become a major direction in armor protection because it dissipates jet energy through multiple mechanisms. Nano-quartz sand is an attractive granular filler, but its physical and mechanical properties change markedly upon water absorption, which in turn alters its resistance to penetration. The relationship between mass moisture content and protective performance in unsaturated water-bearing nano-quartz sand, however, remains unclear. Here, an analytical penetration model was developed from virtual-origin theory and a modified Bernoulli equation, in which an inertial correction coefficient was introduced to represent the equivalent dynamic impedance of the water-bearing granular medium. Static detonation tests were then performed on nano-quartz sand composite targets with mass moisture contents of 5–30 % using a Ø56 mm standard shaped charge, and the penetration depth in the witness target and the comprehensive protection coefficient were measured. The anti-penetration performance varied nonlinearly with mass moisture content, first increasing markedly and then decreasing gradually. Protection peaked at 20 %, where the residual penetration depth was 77 mm and the comprehensive protection coefficient reached 3.46. These results clarify how moisture governs the protective efficiency of granular composite armor and provides a basis for its mixed design.

Keywords: Shaped charge jet; Nano-quartz sand composite target; Moisture content; Penetration resistance

Introduction

The development of shaped charges has substantially reduced the cost-effectiveness of improving protection solely by increasing armor thickness, and it can hardly meet the lightweight requirements of armored equipment. Armor performance is therefore improved by modifying the structural configuration. In composite armor, the impedance mismatch between ceramics, fibers and metals disperses the jet energy[1]; in reactive armor, a sandwiched explosive charge drives flyer plates that disrupt the

jet[2,3]. However, ceramics are brittle, offer poor multi-hit resistance and are restricted by sintering size, while reactive armor causes pronounced collateral damage. Granular-filled armor has thus become one of the most important directions in armor development: when the jet tip strikes hard particles, it is eroded and blunted on the one hand, and on the other hand the particles flow and rearrange under intense dynamic loading, dissipating energy laterally[4–6]; moreover, such armor requires no sintering, can fill arbitrary cavities, and can be replenished after damage, offering significant application advantages.

Quartz sand is one of the most promising filling media. Its Mohs hardness of about 7 provides effective rigid resistance to the jet tip; its true density of about 2.65 g/cm³ is lower than that of commonly used alumina ceramics, which helps control the areal density; and it is chemically inert, widely available and inexpensive. More importantly, quartz sand exhibits a wide range of particle sizes, allowing the porosity, compaction and acoustic impedance to be tuned over a broad range for matching with the confining layer. In this study, nano-scale quartz sand was selected as the research object: compared with conventional quartz sand, nanoparticles possess a higher specific surface area and a finer pore structure, so that capillary effects become more pronounced under moisture, and liquid bridges and matric suction between particles are stronger[7], while the mesoscopic packing uniformity is also improved, which is expected to yield superior energy dissipation against penetration.

Under unsaturated conditions, the physical state of quartz sand changes markedly. From the impedance perspective, partial filling of the pores with water converts the medium from a gas–solid to a liquid–solid two-phase system, and the equivalent density and acoustic impedance increase with saturation, so that the inertial resistance encountered by the jet within the penetration channel also increases[8]; at the same time, liquid bridges form between particles and generate matric suction, increasing the normal contact forces and the shear strength between particles[9,10], which further enhances the rigid resistance to the jet tip. From the perspective of mobility, capillary suction restricts the rolling, rearrangement and dispersal of particles, thereby weakening the cavity-expansion capability of the jet.

However, research on shaped-charge jet penetration into nano-quartz sand with different mass moisture contents remains scarce: existing studies on jet penetration into granular media mostly concern soil[11], and the protective characteristics and mechanisms of such hard, fine-grained media under moisture are still poorly understood. To address this gap, theoretical analysis and static detonation tests were combined in this work. First, based on the virtual origin theory, an analytical penetration model incorporating a modified Bernoulli equation was established, in which the inertial response of the moist granular medium was fully considered, and a formula for the

maximum penetration depth was derived[12,13]. Subsequently, a Ø 56mm standard conical shaped charge was used to conduct static detonation tests on composite targets filled with nano-quartz sand at mass moisture contents of 5%, 10%, 20% and 30%. Finally, the penetration depth in the witness target and the comprehensive protection coefficient were calculated to quantitatively compare the protective efficiency of the composite targets and to reveal the influence of mass moisture content on the protective performance of nano-quartz sand composite targets as well as its underlying mechanism.

Theoretical Analysis

To simplify the derivation process, the following assumptions are made:

Jet model assumptions:

(1) Linear velocity gradient: the jet obeys the virtual-origin hypothesis, with axial velocity decreasing linearly from head to tail and no inter-element axial force[14–16].

(2) Jet continuity: the jet neither necks nor fractures, and only the head element at the target interface is eroded.

(3) In the calculation, the jet is treated as an ideal inviscid incompressible fluid.

Target medium assumptions:

(1) The sand is an isotropic porous granular medium of uniform mass moisture content; no free water was observed in the mixtures, so all four targets remain unsaturated.

(2) The target resistance is inertia-dominated under hypervelocity impact, so the quasi-static strength term is neglected; the pore-water/particle coupling is lumped into the inertial correction coefficient k.

(3) After the cavity is formed, the inner wall is frictionless, and the remaining jet can pass through without obstruction.

Calculation of virtual origin position

The jet parameters were obtained from a validated LS-DYNA simulation.

The two-dimensional model of the Ø56 mm standard shaped charge, as illustrated in Fig. 1, consists primarily of JH-2 explosive and a shaped charge liner[17].

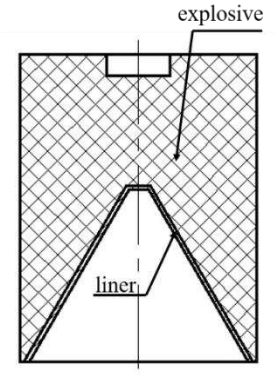

Fig. 1 Two-dimensional model of the Ø56 mm standard shaped charge.

Jet formation was simulated in LS-DYNA with Eulerian meshes.

The parameters for the copper liner (Johnson–Cook + Grüneisen EOS), JH-2 explosive (HEB + JWL EOS), and air (NULL + linear-polynomial EOS) are listed in Supplementary Tables S1–S3[18].

Table 1 Comparison of simulated and experimental results for the Ø56 mm standard shaped charge.

	Experiment[19]	Numerical simulation	Relative error
Time / μs	34	34	0%
Jet morphology			
Jet tip velocity (m/s)	6498	6880	5.9%
Jet tail velocity (m/s)	961	862	10.3%
Tip coordinate/mm		218	
Tail coordinate/mm		48	

As shown in Table 1, the jet morphology from simulations is in good agreement with X-ray test results. The relative errors of jet tip and tail velocities are 5.9% and 10.3%, respectively, verifying the validity of the simulation model. Using the simulation results and virtual origin theory, the virtual origin position is calculated via equation (1).

$$x_0 = \frac{v_{\max} x_2 - v_s x_1}{v_{\max} - v_s} \tag{1}$$

where $v_{\max}$ denotes the velocity of the jet tip, v_s denotes the velocity of the jet

tail, x_1 denotes the coordinate of the jet tip, and x_2 denotes the coordinate of the jet tail.

Theoretical analysis of maximum penetration depth

The Bernoulli equation is applied at the jet penetration interface, and the result is given by equation (2)[20,21].

$$\frac{1}{2}\rho_j(v_j-u)^2=\frac{1}{2}k(\omega)\rho_t(\omega)u^2 \tag{2}$$

where ρ_j denotes the jet density, ω denotes the mass moisture content of nano-quartz sand, u denotes the jet penetration velocity, and v_j denotes the jet velocity. $k(\omega)$ denotes the inertial correction coefficient (lumping inter-particle friction and pore-water pressure coupling into an equivalent impedance), and $\rho_t(\omega)$ represents the density of water-bearing nano-quartz sand, as calculated by equation (5)

The penetration velocity u derived from the above equation is given in equation (3).

$$u=\frac{\sqrt{\rho_j}v_j}{\sqrt{\rho_j}+\sqrt{k(\omega)\rho_t(\omega)}} \tag{3}$$

λ is defined as:

$$\lambda=\frac{\sqrt{\rho_j}}{\sqrt{\rho_j}+\sqrt{k(\omega)\rho_t(\omega)}} \tag{4}$$

The jet penetration velocity satisfies $u=v_j\lambda$.

$$\rho_t(\omega)=\rho_d(1+\omega),0\le\omega\le\omega_{\mathrm{sat}} \tag{5}$$

where ρ_d is the dry sand density; water only fills pores with no volumetric expansion.

Let $t_0=0$ denote the instant at which the jet departs from the virtual origin. The travel time of the leading jet element to the target surface t_1 is given by the equation (6).

$$t_1=\frac{z}{v_{\max}} \tag{6}$$

$$z=h+H-x_0 \tag{7}$$

where z denotes the distance from the virtual origin to the target plate, $v_{\max}$ denotes the velocity of the leading jet element, h denotes the charge height, and denotes the standoff distance.

For an arbitrary time instant t (where $t=0$ is defined as the moment when the leading jet element reaches the target surface), the jet element at the bottom of the penetration crater covers a total travel distance of $z+P(t)$ over an elapsed time of t_1+t. The velocity of this element is thus given by equation (8).

$$v_j=\frac{z+P(t)}{t+t_1} \tag{8}$$

where $P(t)$ denotes the penetration depth at time instant t.

$$\frac{dP}{dt} = u = \frac{z+P(t)}{t+t_1} \cdot \lambda \tag{9}$$

To simplify the solution of the equation, an auxiliary variable $y = z + P$ is introduced. Differentiating with respect to time yields:

$$\frac{dy}{dt} = \frac{dP}{dt} \tag{10}$$

Substituting this into the governing equation gives:

$$\frac{dy}{y} = \frac{\lambda}{t+t_1} dt \tag{11}$$

Integrating both sides and applying the initial condition that $P = 0$ at $t = 0$, corresponding to $y(0) = z$, the solution is obtained as:

$$\frac{z+P}{z} = (\frac{t+t_1}{t_1})^{\lambda} \tag{12}$$

$$P = z(\frac{t+t_1}{t_1})^{\lambda} - z \tag{13}$$

The jet penetration process ceases when the velocity of the jet element at the penetration interface decreases to the effective cutoff velocity, below which no effective penetration can be generated. Let $v_{c,\text{eff}}$ represent the effective cutoff velocity, t_{end} the corresponding termination instant, and P_{max} the maximum penetration depth. Then

$$v_{c,\text{eff}} = \frac{z+P_{\max}}{t_{end}+t_1} \tag{14}$$

The maximum penetration depth of the jet into water-bearing nano-quartz sand P_{max} is given by equation (15).

$$P_{\max} = z\left[\left(\frac{v_{c,\text{eff}}}{v_{\max}}\right)^{\frac{\lambda}{\lambda-1}} - 1\right] \tag{15}$$

Experimental Setup and Results

Experimental Setup

The granular filler used in the tests was nano-quartz sand with an average particle size below 100 nm, which behaved as a nearly continuous powder medium, as shown in Fig. 2.



Fig. 2 Nano-quartz sand powder used in the experiments.

The main frame of the target was machined from high-strength 45# steel, which ensured structural integrity under high-velocity impact and mimicked the base material of real armored vehicle hulls. The frame was a rectangular cuboid with overall dimensions of 145 mm × 145 mm × 90 mm. To prevent lateral leakage of quartz sand during impact, oil-resistant rubber rectangular sealing rings were fitted into the rectangular grooves along the top edge of each cell. A thick cover plate was then assembled and fastened by eight high-strength M8 bolts around the perimeter to apply preload and guarantee sealing. This design ensured that the impact load was mainly borne by the sand layer and the back plate, avoiding lateral pressure relief. The dimensional schematic and photograph of the fabricated composite target are presented in Fig. 3.

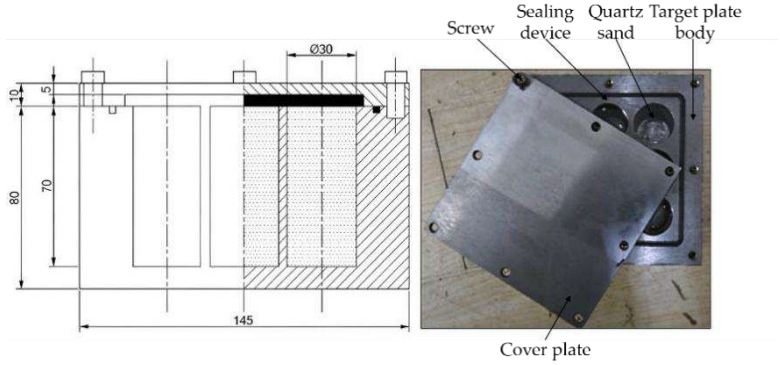

Fig. 3 Schematic diagram and photograph of the composite target.

Penetration experiments on nano-quartz sand composite targets with varying mass moisture contents were conducted using a Ø56 mm standard shaped charge. The influence of mass moisture content on the protective performance of the composite targets was characterized by the residual penetration depth into the witness target.

Four groups of composite targets with mass moisture contents of 5%, 10%, 20% and 30% were designed for the tests. The nano-quartz sand features an ultrafine particle size and powdery morphology and forms a suspension or paste when mixed with water. In particular, the mixtures with 20% and 30% mass moisture content exhibited a distinct colloidal state. All mixtures were uniformly stirred prior to filling to ensure a consistent state. A total of five shots were carried out: one baseline penetration test on 45# steel using the Ø56 mm standard shaped charge, and four penetration tests on composite targets with different mass moisture contents.

The test arrangement is shown in Fig. 4. The shaped charge was mounted on the No. 1 standoff tube, with its axis precisely aligned with the center of the composite target. The nano-quartz sand composite target was placed on the No. 2 standoff tube, which was positioned above the witness target. The No. 1 stand-off tube had a height of 80 mm, and the No. 2 stand-off tube had a height of 90 mm, ensuring that the penetration result of the witness target was not affected by back-face spallation from

the composite target. The witness target was made of 45# steel with a thickness of 200 mm.

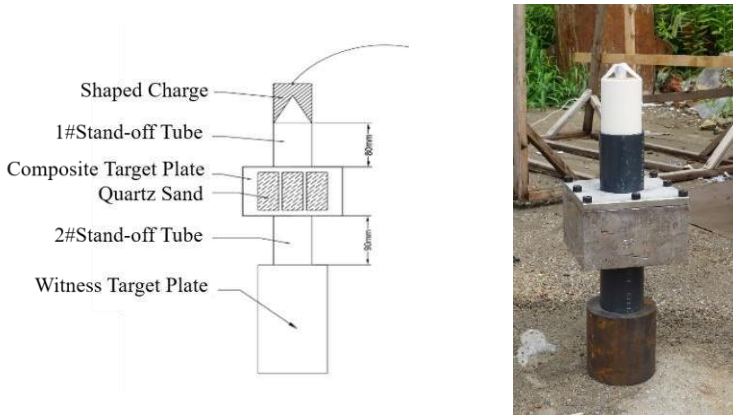

(a) Experimental layout schematic

(b) Site photograph of static detonation test for composite target plates

Fig. 4 Schematic diagram and photograph of the experimental arrangement.

Experimental Results

The results of the five firing tests are presented in Fig. 5. The baseline penetration depth of the Ø56 mm standard shaped charge into a 400 mm-thick 45# steel block was measured as 225.4 mm. Detailed data of the residual penetration depth in the witness target for composite targets with varying mass moisture contents are provided in Table 2.

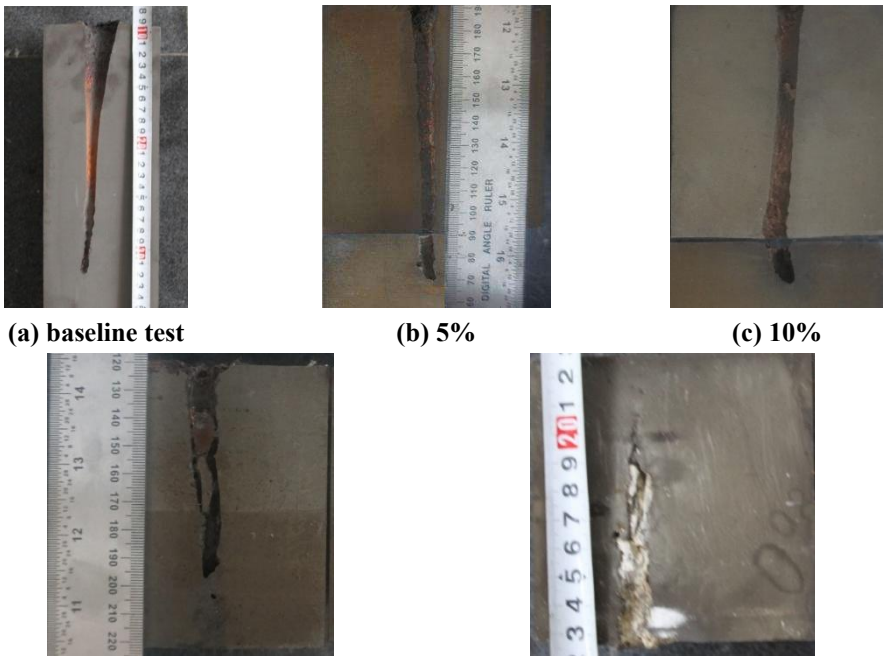

(a) baseline test **(b) 5%** **(c) 10%**

(d) 20% **(e) 30%**

Fig. 5 Test results of the baseline test and composite targets with 5%, 10%, 20% and 30% mass moisture content.

Table 2 Test results of composite targets with different mass moisture contents.

Test No.	Mass moisture content of composite target (mass fraction)	Residual penetration depth in witness target / mm
#1	5%	120
#2	10%	114
#3	20%	77
#4	30%	85

The test results indicate that the anti-penetration performance of water-bearing nano-quartz sand composite targets against shaped charge jets does not follow a monotonic trend with mass moisture content but presents a complex nonlinear variation pattern. Under the test conditions, the composite target with 20% mass moisture content delivered the best protective effect, with a residual penetration depth of only 77 mm in the witness target. As the mass moisture content rose to 30%, the protective performance declined slightly, and the residual penetration depth increased to 85 mm. The protective capacity of the 10% and 5% mass moisture content specimens decreased successively, which indicated the existence of an optimal mass moisture content range.

The comprehensive protection coefficient E was adopted to quantitatively assess the overall protective performance of the nano-quartz sand composite targets, and its calculation formula is expressed as equation (16)[22].

$$E = N \cdot N_b \tag{16}$$

$$N = \frac{(T_b - T_{wp})\rho_s}{\delta_t \rho_t} \tag{17}$$

$$N_b = \frac{T_b - T_{wp}}{\delta_t} \tag{18}$$

where N is the mass protection coefficient, N_b is the thickness protection coefficient, T_b is the baseline penetration depth of the shaped charge, T_{wp} is the residual penetration depth after jet penetration through the composite target, ρ_s is the density of steel, δ_t is the thickness of the composite target, and ρ_t is the average density of the composite target.

Table 3 Calculated protective efficiency of nano-quartz sand composite targets with different mass moisture contents.

Mass moisture content (mass fraction)	Total mass of target/kg	Mass of target housing/kg	Average density$\rho_t(kg/m^3)$	Mass protection coefficient (N)	Thickness protection coefficient (N_b)	Comprehensive protection coefficient (E)
5%	11.485	10.78	6069.49	1.51	1.17	1.77
10%	11.544	10.78	6100.67	1.59	1.24	1.97

Mass moisture content (mass fraction)	Total mass of target/kg	Mass of target housing/kg	Average density$\rho_t(kg/m^3)$	Mass protection coefficient (N)	Thickness protection coefficient (N_b)	Comprehensive protection coefficient (E)
20%	11.618	10.78	6139.78	2.10	1.65	3.46
30%	11.683	10.78	6174.13	1.98	1.56	3.09

As can be observed from the calculation results in Table 3, the comprehensive protective performance (E) of the composite target exhibited a nonlinear trend of significant increase followed by a slight decrease with rising mass moisture content. The target achieved the optimal protective efficiency at a mass moisture content of 20% and the comprehensive protection coefficient (E) was 3.46. However, when the mass moisture content increased to 30%, the comprehensive protection coefficient (E) dropped to 3.09.

Discussion

To reveal the underlying mechanism governing this nonlinear protective performance variation, the evolution of physical state and inter-particle interaction of the nano-quartz sand medium with increasing mass moisture content was analyzed in detail. As the mass moisture content increases gradually from the dry state, the physical state and anti-penetration energy dissipation capacity of nano-quartz sand follow a nonlinear trend of initial strengthening followed by weakening. This phenomenon is essentially attributed to the gradual transition of water occurrence states from surface adsorbed water to capillary water and free water, which drives the evolution of inter-particle forces. In the dry state, nano-sized particles are loosely packed and bound only by weak van der Waals forces, leading to low cohesion and the poorest protection performance. At low mass moisture contents, adsorbed water films form on particle surfaces and create capillary liquid bridges, which rapidly improve the cohesion of the sand matrix and significantly enhance its protection performance. In the medium mass moisture content range, the capillary bonding effect reaches its peak, and the coupled energy dissipation from particle friction and pore water pressure achieves the highest efficiency, corresponding to the optimal protection performance. As mass moisture content continues to increase, excess water pushes particles apart and weakens inter-particle contact friction, causing the sand matrix to gradually transition to a slurry state, with both cohesion and overall protection performance decreasing progressively.

To quantify this moisture dependence and to close the analytical model, the inertial correction coefficient $k(\omega)$ was back-calculated from the four tests. Jet penetration was terminated at a cutoff velocity below which the jet no longer penetrates; with the nominal cutoff of 2250 m/s, the ideal model over-predicted the baseline by 21.1%, so

an effective cutoff velocity of 2531 m/s, calibrated against the baseline test, was adopted to absorb the effect of jet particulation[23]. Tracking the jet through the layered target (5 mm steel cover, 5 mm rubber seal, 70 mm sand, 10 mm steel back plate) with the modified Bernoulli relation of equation (2) and stopping at the cutoff, $k(\omega)$ was determined at each mass moisture content by matching the measured residual penetration depth. The coefficient rose from 1.31 at 5% to a peak of 3.86 at 20% and then declined to 2.94 at 30%, confirming 20% as the optimal mass moisture content. Detailed values of $k(\omega)$ are provided in Supplementary Table S4.

Conclusions

In this study, a theoretical model for shaped charge jet penetration into water-bearing nano-quartz sand composite targets was established based on the virtual origin theory and the modified Bernoulli equation, and the analytical expression for maximum penetration depth was derived. The anti-penetration performance of nano-quartz sand composite targets with mass moisture contents of 5%, 10%, 20% and 30% was systematically investigated through static detonation tests. The main conclusions are drawn as follows:

(1) The anti-penetration performance of water-bearing nano-quartz sand composite targets against shaped charge jets varies nonlinearly with mass moisture content, and an optimal mass moisture content exists within the test range. Within the 5%–30% mass moisture content interval, the comprehensive protection coefficient of the target first increases markedly and then decreases gradually with rising mass moisture content. The optimal protective performance occurs at 20% mass moisture content, with a residual penetration depth of only 77 mm in the witness target and a comprehensive protection coefficient of 3.46, representing a nearly two-fold improvement compared with the 5% mass moisture content condition. As the mass moisture content rises to 30%, the protective effect shows a slight decline.

(2) A theoretical model for shaped charge jet penetration into water-bearing granular media was constructed. The calculation formula for maximum penetration depth was derived based on the virtual origin theory and the interfacial Bernoulli equation. An inertial correction coefficient was introduced to characterize the influences of non-ideal flow effects, including inter-particle friction and pore water pressure coupling, on penetration depth.

(3) The inertial correction coefficient of water-bearing nano-quartz sand was back-calculated based on the penetration model with a cutoff velocity of 2531 m/s. The coefficient rose from 1.31 at a mass moisture content of 5% to a peak value of 3.86 at 20%, and then decreased to 2.94 at 30%. The calibrated coefficient can serve as a quantitative reference for the mix proportion design of water-bearing granular

composite armor.

Data availability statement

The datasets generated and/or analysed during the current study are available from the corresponding author on reasonable request.

References

1. Chen, Z. *et al.* Analysis of bulletproof performance of structurally optimized ceramic composite armor through numerical simulation and live fire test. *Sci. Rep.* **14**, (2024).
2. Fras, T. Experimental and numerical study on a non-explosive reactive armour with the rubber interlayer applied against kinetic-energy penetrators-the 'bulging effect' analysis. *Materials* **14**, 3334 (2021).
3. Mayseless, M., Friling, S. & Misiuk, L. Re-visiting the mass-flux model for explosive reactive armor and the effect of plate thickness. *Def. Technol.* **17**, 779–785 (2021).
4. Ahmed, Mohd., AlQadhi, S., Mallick, J., Desmukh, M. N. & Hang, H. T. Advances in projectile penetration mechanism in soil media. *Applied Sciences* **10**, 6810 (2020).
5. Omidvar, M., Iskander, M. & Bless, S. Response of granular media to rapid penetration. *Int. J. Impact Eng.* **66**, 60–82 (2014).
6. Miyai, S., Kobayakawa, M., Tsuji, T. & Tanaka, T. Influence of particle size on vertical plate penetration into dense cohesionless granular materials (large-scale DEM simulation using real particle size). *Granular Matter* **21**, (2019).
7. Luo, J. *et al.* Molecular dynamics analysis of wetting behavior of nano water drops on quartz sand surface. *C. R., Mec.* **349**, 485–499 (2021).
8. Lin, J., Zhao, T. & Jiang, M. Investigating projectile penetration into immersed granular beds via CFD-DEM coupling. *Granular Matter* **25**, (2023).
9. Fredlund, D. G., Morgenstern, N. R. & Widger, R. A. The shear strength of unsaturated soils. *Can. Geotech. J.* **15**, 313–321 (1978).
10. Daman Shokouh, A., Nikooe, E. & Habibagahi, G. Effects of dynamic capillarity on the shear strength of sandy soils during transient two-phase flow. *Vadose Zone J.* **23**, e20240032 (2024).
11. Shi, G. & Huang, Z. Theoretical and experimental study of shaped charge jet penetration into frozen soil at different temperatures. *Lat. Am. J. Solids Struct.* **23**, e9061 (2026).
12. Liu, B., Huang, Z. X. & Zu, X. D. Spaced armor effects on shaped charge jet penetration. *Propellants, Explos., Pyrotech.* **39**, 859–866 (2014).
13. Birkhoff, G., MacDougall, D. P., Pugh, E. M. & Taylor, G. Explosives with lined cavities. *J. Appl. Phys.* **19**, 563–582 (1948).
14. Jiang, K., Deng, S. C. & Li, H. B. Theoretical calculation and analysis of the velocity of shaped charge jet with modified collapse velocity model. *Pet. Sci.* **21**, 4311–4327 (2024).
15. Walters, W. P. & Zukas, J. A. Fundamentals of shaped charges. *(No Title)* (1989).
16. Abrahamson, G. & Goodier, J. Penetration by shaped charge jets of nonuniform velocity. *J. Appl. Phys.* **34**, 195- (1963).
17. Ma, B. *et al.* Investigate the effects of magnetic fields on the penetration ability of a shaped charge jet at different standoffs. *Def. Technol.* **17**, 1722–1730 (2021).
18. Chen, S. M. Study on Shock Initiation Mechanism of Moving Cased Charge under Jet Impact. (Nanjing University of Science and Technology, Nanjing, China, 2022).
19. Song, P., Li, W., Liu, J., Zhang, Q. & Wang, Z. Research on plastic flow characteristic parameter distribution of shaped-charge jet: theory, experiment, and simulation. *Appl. Sci.* **13**, 5128 (2023).
20. Pugh, E. M., Eichelberger, R. J. & Rostoker, N. Theory of jet formation by charges with shallow conical liners. *Journal of Applied Physics* **23**, 532–538 (1952).
21. Xiao, Q., Huang, Z., Zu, X., Jia, X. & Ma, B. The effects of compressibility and target strength on shaped charge jet penetration. *Def. Technol.* **56**, 244–253 (2026).
22. Cao, H. Q., Sun, B. S, & Xu, L. T. *Research on Armor Protection Technology*. (Beijing Institute of Technology Press, Beijing, China, 2019).
23. Ugri\vciæ, M. Determination of the critical jet velocity during the penetration into the homogenous

steel obstacle. in (2003).

Funding

This work was supported by the Open Research Fund of the State Key Laboratory of Target Vulnerability Assessment, Defense Engineering Institute, Academy of Military Sciences (AMS), grant number YSX2024KFXY005.

Author contributions

Conceptualization, S.W. Chen and M Xia; Methodology, H Wang, S.W. Chen and M Xia; Investigation, H Wang and Z.G. Ding; Writing – original draft, H Wang; Writing – review & editing, S.W. Chen and M Xia; Funding acquisition, M Xia; Supervision, M Xia; Validation, M Xia and Z.G. Ding.

Competing interests

The authors declare no competing interests.

Supplementary Files

This is a list of supplementary files associated with this preprint. Click to download.

- Supplementary.docx